A LOW REYNOLDS *k*-ε MODEL FOR VISCOELASTIC FLUIDS

D. O. A. Cruz and C. E. Maneschy
Departamento de Engenharia Mecânica, Universidade Federal do Pará- UFPa, Campus Universitário do Guamá, 66075-900, Belém, Pará, Brasil
doac@ufpa.br

F. T. Pinho
Centro de Estudos de Fenómenos de Transporte, DEMEGI, Faculdade de Engenharia, Universidade do Porto, Rua Dr. Roberto Frias s/n, 4200-465 Porto, Portugal
fpinho@fe.up.pt

Abstract. *A low Reynolds number $k-\varepsilon$ model was developed for predicting drag reducing turbulent flows of elastic fluids. The rheology of the fluid was modelled by a Generalized Newtonian model modified to mimic relevant effects of extensional viscosity. A new damping function, that takes wall effects into account, is also proposed. The predictions of friction factor, mean velocity and turbulent kinetic energy compare favourably with data from the literature for various polymer solutions. The advantage of this model is that it only needs input data from the rheology of the fluid and the bulk velocity of the flow in contrast to existing models for drag reducing fluids which must be modified on a case by case basis*.

Keywords*. Drag reduction, pipe flow, viscoelastic fluid, turbulence modeling, $k-\varepsilon$ model*

1. Introduction

The development of turbulence models for engineering applications in duct flows of drag reducing fluids has not received the attention it deserves. Early work took place in the 1970s (Mizushina et al, 1974; Hassid and Poreh, 1975; Durst and Rastogi, 1977) and later attempts were usually limited to inelastic fluids (Malin, 1997; Cruz et al, 2000). The existing turbulence models usually consist of the Newtonian formulation with *ad-hoc* modifications, especially in the numerical value of the parameters. These depend on the fluid and flow to be predicted and do not take full account of fluid rheology. A more detailed review can be found in Pinho (2003).

Adopting a Generalised Newtonian fluid (GNF) which was modified to include effects of strain-hardening of the extensional viscosity, Pinho (2003) derived the transport equations of momentum, Reynolds stress, turbulent kinetic energy and its rate of dissipation and then performed an order of magnitude analysis to identify their relevant terms. That work then concentrated on developing closure for a $k-\varepsilon$ type model, but no details were given of the numerical values of the parameters and of the form of the damping functions and no predictions were carried out or comparisons made with experimental data. The present work completes the task by providing those missing details, performing simulations of pipe flow with viscoelastic polymer solutions and comparing the corresponding results with experimental data.

The paper is organised as follows: in the next section the equations to be solved and the turbulence model are presented. The results of the simulations and their comparison with experimental data is the subject of Section 3. The paper ends with a summary of the main conclusions and a list of future developments.

2. Rheological and transport equations

2.1. The fluid constitutive equation

The generalised Newtonian fluid (GNF) of Eq. (1) is adopted where the viscosity function is given by Eq. (2)

$$\sigma = 2\mu \mathbf{S} \tag{1}$$

$$\mu = \eta_v \times K_e \left[\dot{\varepsilon}^2\right]^{\frac{p-1}{2}} \quad \rightarrow \quad \mu = K_v \left[\dot{\gamma}^2\right]^{\frac{n-1}{2}} K_e \left[\dot{\varepsilon}^2\right]^{\frac{p-1}{2}} \tag{2}$$

This expression combines shear-thinning and strain-hardening, the latter in an attempt to mimic the effect of extensional viscosity on turbulent flow, as explained in Pinho (2003). The first part of Eq. (2) accounts for the viscometric behaviour where the consistency and power law indices (K_v and n) are obtained by least-square fitting to viscometric viscosity data. The second part of Eq. (2) introduces the strain-rate dependence into the viscosity model, while respecting some physical constraints and homogeneity. It must obey some limiting behaviours and consequently it is given as the following ratio of extensional (η_e) and viscometric (η_v) viscosities

$$\frac{1}{3}\frac{\eta_e(\dot{\varepsilon})}{\eta_v(\dot{\gamma})} = K_e\left[\dot{\varepsilon}^2\right]^{\frac{p-1}{2}} \tag{3}$$

The 1/3 coefficient ensures that, for purely viscous fluids, the viscometric behaviour is fully recovered in the limit of very small deformations, in agreement with continuum mechanics. This ratio must be calculated at $\dot{\gamma} = \sqrt{3}\dot{\varepsilon}$ for reasons explained in Barnes et al (1989). We recommend that the experimental data for the extensional viscosity be fitted by a power law, and then divided by $3K_v\left|\sqrt{3}\dot{\varepsilon}\right|^{n-1}$, in this way providing both the coefficient K_e and index p. $\dot{\varepsilon}$ stands for an invariant of the rate of deformation tensor measuring the strain rate (Pinho, 2003).

The viscosity is a non-linear function of fluctuating kinematic tensors and so it is decomposed into average and fluctuating viscosities. An expression for the time-average molecular viscosity was derived in detail by Pinho (2003) and is given by Eq. (4). The expression is in closed form once the turbulence kinetic energy $k \equiv \overline{u_{ii}^2}/2$ and its rate of dissipation ε are known.

$$\overline{\mu}_h = \left(C_\mu \rho\right)^{\frac{3m(m-1)A_2}{8+3m(m-1)A_2}} 2^{\frac{4m(m-1)A_2}{8+3m(m-1)A_2}} k^{\frac{6m(m-1)A_2}{8+3m(m-1)A_2}} \varepsilon^{\frac{[8-3(m-1)A_2]m}{8+3m(m-1)A_2}} B^{\frac{8}{8+3m(m-1)A_2}} \tag{4}$$

with $A_2 = 0.45$, $A_\varepsilon = 10$ and m and B are given by

$$m \equiv \frac{n+p-2}{n+p} \qquad \text{and} \qquad B = \left[\frac{K_v K_e}{A_\varepsilon^{p-1}}\right]^{1-m} 2^{\frac{(n-1)-m(n+1)}{2}} \rho^m \tag{5}$$

The effect of turbulence on the average molecular viscosity $\overline{\mu}_h$, via the nonlinear dependence on $\dot{\gamma}$ and $\dot{\varepsilon}$, appears through the two terms of Eq. (4) containing k and ε. If the fluid has no shear-rate and no strain-rate dependence, a constant viscosity coefficient $\overline{\mu}_h = K_v K_e$ is recovered.

Since expression (4) was derived from arguments of high Reynolds number turbulence (subscript h), the true average molecular viscosity in near-wall regions cannot be exclusively given by $\overline{\mu}_h$. At a wall there will be no velocity fluctuations, the flow will be one-dimensional, and the average viscosity must reduce to a pure viscometric form without any extensional effect . To take this into account the average molecular viscosity $\overline{\mu}$ is given by

$$\overline{\mu} = f_v\overline{\mu}_h + (1 - f_v)\eta_v \tag{6}$$

introducing the damping function f_v. The role of f_v is akin to that of the damping function for the eddy viscosity f_μ and it was decided by Cruz and Pinho (2003) to make $f_v = f_\mu$ after an extensive series of tests. The function f_μ is presented in Section 2.2.

2.2. Transport equations

For fully-developed pipe flow the transport equation of momentum is

$$0 = \frac{1}{r}\frac{d}{dr}\left[r\left(\overline{\mu}\frac{dU}{dr} - \rho\,\overline{uv}\right)\right] - \frac{d\overline{p}}{dx} \tag{7}$$

where r is the radial coordinate, x is the longitudinal coordinate, U is the axial mean velocity and $\overline{p}$ is the time-average pressure. The Reynolds shear stress is given by the turbulent viscosity hypothesis (Eq. 8) and the eddy viscosity ν_T is modeled by the Prandtl- Kolmogorov equation, dampened by f_μ to account for low Reynolds number effects.

$$-\rho\,\overline{uv} = \rho\nu_T\frac{\partial U}{\partial r} \;\rightarrow\; -\rho\,\overline{uv} = \rho C_\mu f_\mu \frac{k^2}{\tilde{\varepsilon}}\frac{\partial U}{\partial r} \tag{8}$$

Eq. (8) uses the modified rate of dissipation $\tilde{\varepsilon}$ of turbulent kinetic energy, as is typical in most near-wall low Reynolds number k-ε models (Patel et al, 1985), to facilitate the implementation of wall boundary conditions. It is related to the true rate of dissipation ε by $\varepsilon = \tilde{\varepsilon} + D$, where D is the last term on the right-hand-side of Eq. (9). k and $\tilde{\varepsilon}$ are obtained from their own transport equations for fully-developed pipe flow (Eqs 9 and 10). For viscoelastic fluids the transport equation of k was proposed by Pinho (2003).

$$0=\frac{1}{r}\frac{d}{dr}\left[r\left(\frac{\bar{\mu}}{\rho}+\frac{\nu_T}{\sigma_k}\right)\frac{dk}{dr}\right]-\overline{uv}\frac{\partial U}{\partial r}-\tilde{\varepsilon}+2\bar{\nu}\left(\frac{\partial\sqrt{k}}{\partial r}\right)^2 \tag{9}$$

$$0=\frac{1}{r}\frac{d}{dr}\left[r\left(\bar{\mu}+\rho\frac{\nu_T}{\sigma_\varepsilon}\right)\frac{d\tilde{\varepsilon}}{dr}\right]+\rho f_1 C_{\varepsilon 1}\frac{\tilde{\varepsilon}}{k}P-\rho f_2 C_{\varepsilon 2}\frac{\tilde{\varepsilon}^2}{k}+\bar{\nu}\bar{\nu}_T\left(1-f_\mu\right)\left(\frac{\partial^2 U}{\partial r^2}\right)^2+C_{\varepsilon 3}\frac{\nu_T}{\sigma_E\bar{\nu}}\frac{d\tilde{\varepsilon}}{dr}\frac{d\bar{\mu}}{dr} \tag{10}$$

There are several low Reynolds number k-ε models for Newtonian fluids which differ in the numerical values of their parameters and in the form of their damping functions (Patel et al, 1985). As explained in Cruz and Pinho (2003), this turbulence model is based on Nagano and Hishida's (1987) model for Newtonian fluids where the damping functions f_1, f_2 and f_μ take on the following forms:

$$f_1=1.0,\quad f_2=1-0.3\exp\left(-R_T^2\right)\ \text{with}\ R_T=\frac{k^2}{\bar{\nu}\tilde{\varepsilon}}\ \text{and}\quad f_\mu=\left[1-\exp\left(-y^+/26.5\right)\right]^2 \tag{11}$$

The modifications to the Newtonian low Reynolds number k-ε turbulence model are of two types:

i) Direct changes in the equations due to a different constitutive equation: the new last term on the right-hand-side of Eq. (10), the new time-average molecular viscosity ($\bar{\nu}\equiv\bar{\mu}/\rho$) and its damping function f_ν;

ii) Modifications of existing terms, parameters or damping functions: the new form of damping function f_μ.

The wall coordinate y^+ must use the new time-average molecular viscosity and two definitions, shown in Eq. (12), are possible: the use of the local time-average viscosity, leading to y^+, or of the wall viscosity ($\bar{\nu}_w$) leading to y_w^+. In both cases u_τ represents the friction velocity. The corresponding damping functions f_μ will be referred to as the M1 and M2 formulations, respectively.

$$y^+=\frac{u_\tau y}{\bar{\nu}}\quad\text{or}\quad y_w^+\equiv\frac{u_\tau y}{\bar{\nu}_w} \tag{12}$$

To derive f_μ for this GNF constitutive model, Van Driest's (1956) philosophy was used but adapted to the new fluid rheology. The damping function was considered to be the product ($f_\mu=f_{\mu\nu}f_{\mu e}$) of a purely viscometric contribution ($f_{\mu\nu}$ for p= 1, n < 1) by a purely extensional contribution ($f_{\mu e}$ for p > 1, n = 1). For each contribution we attempted to derive expressions showing the form of the attenuation of oscillations in the second problem of Stokes, as explained in detail in Cruz and Pinho (2003). The final form of the damping function is

$$f_\mu=\left\{1-\left[1+\left|\frac{1-n}{1+n}\right|y^+\right]^{-\left|1+n\right/1-n\right|/A^+}\right\}\times\left\{1-\left[1+\left|\frac{p-1}{3-p}\right|y^+C^{\frac{1-p}{2-p}}\right]^{-\left|3-p\right/p-1\right|/A^+}\right\} \tag{13}$$

with A^+ = 26.5, the value used by Nagano and Hishida (1987). The function introduces parameter C requiring quantification, the subject of Section 3.1. For n = 1 and p = 1, Eq. (13) gives the expression in Eq. (11).

The other coefficients of the model, listed in Table 1, remain unchanged because the amount of data required for their determination for viscoelastic fluids are scarce and the new parameter $C_{\varepsilon 3}$ takes the numerical value of 1 for the same reasons.

Table 1- Values of the parameters assigned to Nagano and Hishida's low Reynolds k-ε model.

C_μ	σ_k	σ_ε	$C_{\varepsilon 1}$	$C_{\varepsilon 2}$
0.09	1.0	1.3	1.45	1.90

3. Results and discussion

To test the two formulations of the turbulence model, predictions must be compared with sets of experimental data that include measurements of the viscometric and extensional viscosities.

Simultaneous measurements of extensional viscosity, viscometric viscosity and hydrodynamic quantities for dilute polymer solutions are scarce in the literature but were carried out by Escudier et al (1999) and Presti (2000). Escudier et al (1999) performed pressure drop, flow rate and LDA measurements of the mean velocity in a pipe flow with a diameter of 100.4 mm, using aqueous solutions of polyacrilamide (PAA), xanthan gum (XG), carboxymethil cellulose

(CMC) and a blend of XG and CMC at various weight concentrations. The corresponding turbulence kinetic energy data are available in Presti (2000).

Fitting Eqs. (2) and (3) to the experimental viscometric and extensional viscosity data yielded the parameters listed in Table 2.

Table 2- Parameters of viscosity law of Eqs. (2) and (3) used to fit the viscosity data in Escudier et al (1999)

Fluid	K_v [Pas^n]	n	K_e	p
0.25% CMC	0.2639	0.6174	2.0760	1.2678
0.3% CMC	0.2748	0.6377	2.7485	1.2214
0.09% CMC/0.09% XG	0.15178	0.5783	2.1833	1.1638
0.2% XG	0.2701	0.4409	3.8519	1.2592
0.125% PAA	0.2491	0.425	1.9394	1.4796

All solutions are shear-thinning and Trouton-thickening, i.e., although the extensional viscosity was found to be strain-thinning, its rate of decrease with strain rate is slower than that of the viscometric viscosity with shear rate and consequently the Trouton ratio is strain-hardening.

A first series of simulations was carried out with the aqueous solution of 0.125% PAA, aimed at determining the value of the new parameter C appearing in the damping function $f_{\mu e}$. This fluid was selected randomly. Then, using only the flow rate and the rheology of the fluids as input conditions, predictions of turbulent flow for other fluids were performed.

The numerical simulations were carried out with a finite volume code and the wall to wall computational domain was represented by a non-uniform mesh with 199 cells having at least 12 control volumes within each viscous sub-layer ($y_w^+ < 5$). This mesh provided mesh-independent results within 0.1%.

3.1. Determination of parameter *C*

The correct strategy for evaluating parameter C would be the solution of an inverse problem, but this was not attempted and a trial-and-error method was used instead. Using the rheology for 0.125% PAA several numerical values of C were tried and the predictions of $f - Re_w$ were compared with the experimental $f - Re_w$ data, where f is Darcy's friction coefficient and Re_w is the Reynolds number based on the wall viscosity and bulk flow velocity.

Figure 1 compares the predictions of $f - Re_w$ with data from Escudier et al (1999). The computations were made with models M1 and M2 of the damping function. M2 gave higher values of the friction coefficient than M1, but in both cases the amount of drag reduction was clearly in excess to that due to purely shear-thinning behaviour represented by the dashed line. The dashed line represents the friction factor for a purely viscous fluid ($p = 1$) obeying the same power law model and is given by Eq. (14) according to Dodge and Metzner (1959). For reference, the maximum drag reduction asymptote (MDRA) of Virk (1975) (Eq. 15) is also plotted.

$$\frac{1}{\sqrt{f}} = 0.8685 n^{0.25} \ln\left(\frac{2n}{3n+1}\mathrm{Re}_w \sqrt{f}\right) + \frac{2.4082}{n^{0.75}}(1-n) - \frac{0.2}{n^{1.2}} \tag{14}$$

$$\frac{1}{\sqrt{f}} = 9.5 \log\left(\mathrm{Re}_w \sqrt{f}\right) - 19.06 \tag{15}$$

For the predictions to compare well with experiments C= 9 is needed for M1. For M2, a higher value of C is required, especially at high Reynolds numbers. Parameter C was introduced in an order of magnitude analysis leading to $f_{\mu e}$ and we feel that it should not differ from 1 by more than a factor of 10. Although C was kept at 9 for both damping functions in this work, the value should be optimised for formulation M2.

The slope of the $f - Re_w$ predictions is less than that for the measurements indicating the need for further improvements in the turbulence model. The figure also includes results of simulations for a similar fluid without strain rate dependence of the Trouton ratio (p= 1). For model M2, these predictions compare well with Eq. (14) showing no elastic drag reduction as it should: at high Reynolds numbers the difference relative to Eq. (14) is of the order of 1% or less whereas at low Reynolds numbers the model predicts a higher value of f by up to 10%. In contrast, M1 predictions for p= 1 have excessive drag reduction, an indication that the M2 formulation is to be preferred, in spite of a less good prediction of the f for viscoelastic fluids. However, this can be improved by increasing the numerical value of C without any impact for p= 1.

The disagreement between the experimental data and the laminar correlation at low Reynolds numbers ($fRe = 64$) is due to different scalings. The data are plotted here using the wall Reynolds number, whereas the correlation f= 64/Re is universal when using the generalised Reynolds number.

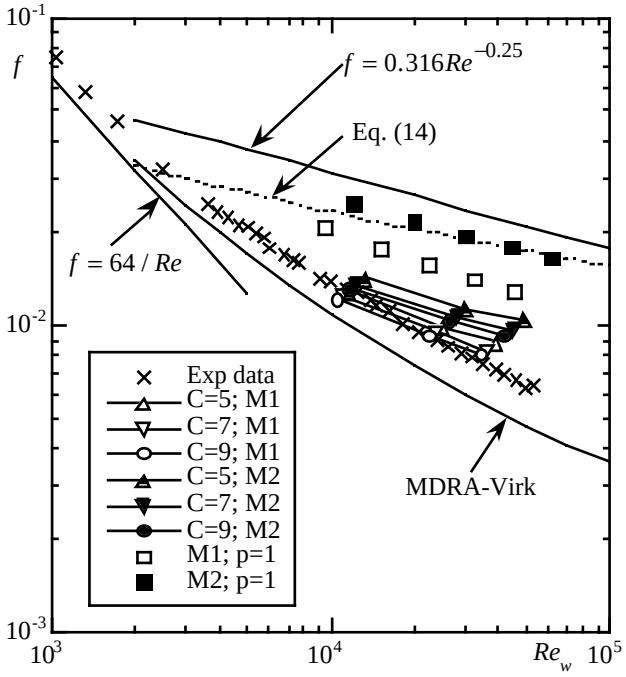

Figure 1- Comparison between the predicted and experimental (Escudier et al, 1999) *fRe* for 0.125% PAA. Open symbols (M1) refer to Model 1, closed symbols (M2) refer to Model 2. *p*=1 refers to simulations for purely viscous 0.125% PAA solution.

3.2. Friction factor

Using *C*= 9, predictions of *f* for the other fluids are compared in Fig. (2). The figure shows mixed results: M2 always predicts less drag reduction than M1, but the difference is particularly large for the 0.2% XG solution (in excess of 30%) and less so for the blend of CMC and XG (20%). With the other fluids the predictions of drag reduction (DR) with M2 are about 15% lower than those obtained by M1. Drag reduction (DR) is defined as

$$DR = \frac{f - f_N}{f_N} \times 100\% \tag{16}$$

where f_N is the Newtonian friction factor at identical Reynolds number. Of significance was the fact that in all cases drag reduction was significantly larger than the amount exclusively attributed to shear-thinning (Eq. 14).

Model M1 predicted well the results for 0.25% CMC and the blend (at low Reynolds numbers) and slightly overpredicted drag reduction for the 0.3% solution. Model M2 predicted well the drag reduction for 0.3% CMC and 0.25% CMC at low Reynolds numbers and underpredicted in the other cases. In all cases the slope of $f - Re_w$ was lower than the slope of the measured $f - Re_w$ data, hence the agreement between predictions and experiments is always over a limited range of Reynolds numbers. Still, it is important to emphasize that this is the first time a general turbulence model, not previously tuned with the flows to be predicted, has been able to calculate such intense drag reductions in turbulent viscoelastic pipe flow.

3.3. Mean velocity

Figure 3 compares predicted mean velocity profiles in wall coordinates with measured data from Escudier et al (1999). Other cases are not shown here for conciseness, but the comparisons are qualitatively identical.

The figures include several curves: the Newtonian log-law profile, the viscous sub-layer velocity profile and Virk's (1975) ultimate drag reduction asymptote. Figure 3-a) also includes predictions for a Newtonian fluid ($n= p = 1$) at a high Reynolds number of 200,080 obtained with the same code and turbulence model. The Newtonian prediction collapses with the viscous sub-layer equation for $y_w^+ < 4$ and is in agreement with a standard Newtonian log-law expression for $y_w^+ > 40$. This confirms the generality of the proposed turbulence model.

The experimental profiles show three regions in agreement with Virk (1975): the viscous sub-layer at low values of y_w^+, an inertial layer at high y_w^+ with the same slope as the Newtonian log-law, and an intermediate log-law layer with a higher slope than the inertial sub-layer. For very large drag reductions the intermediate log-law extends through the whole pipe.

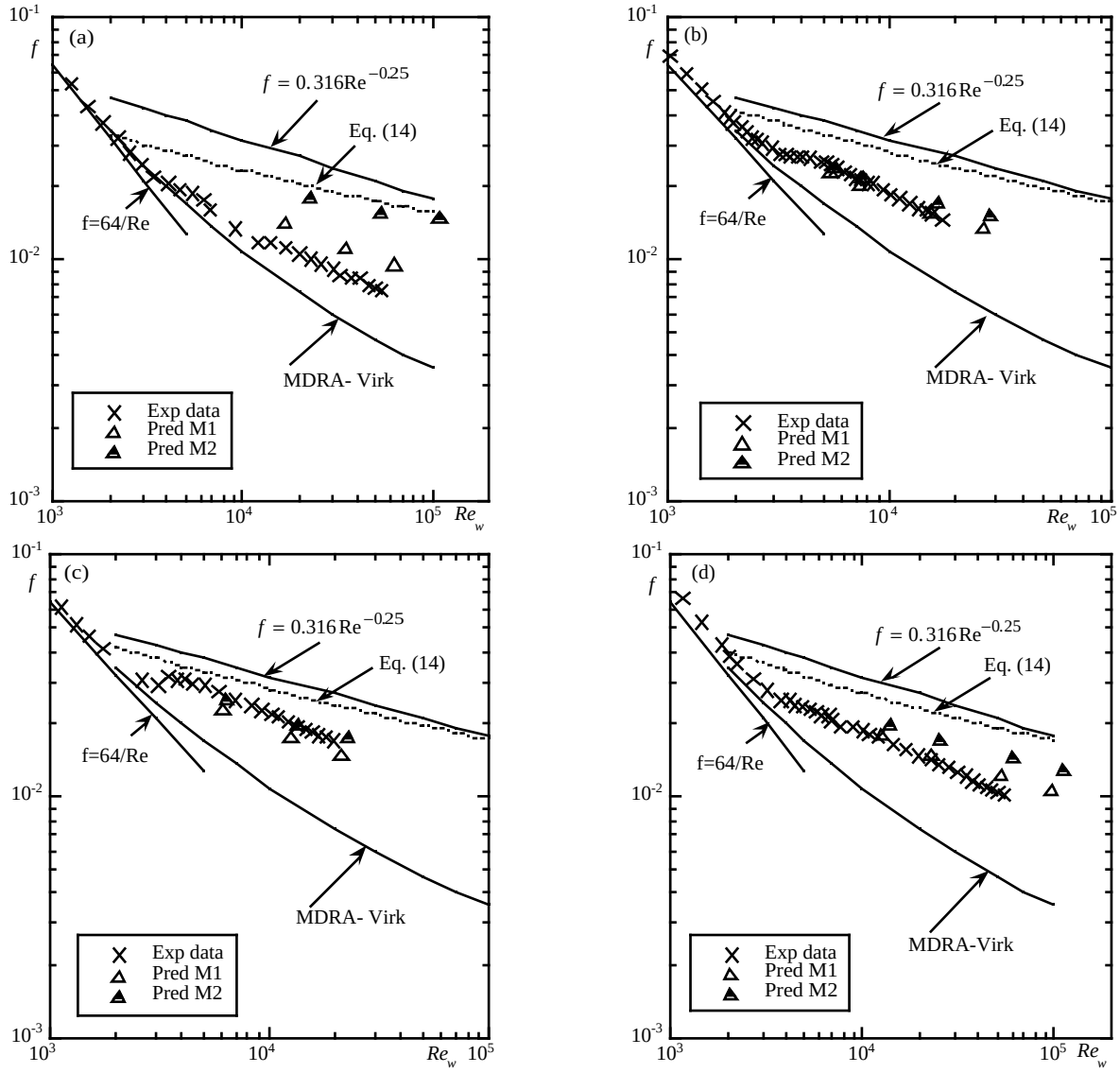

Figure 2- Comparison between predicted and measured *fRe* [9] for various polymer solutions: (a) 0.2% XG; (b) 0.25% CMC; (c) 0.3% CMC; (d) 0.09%/0.09% CMC/XG blend.

The comparisons between the non-Newtonian predictions and the experiments are remarkable considering the novelty of the turbulence model. The turbulence model captures the viscous sub-layer and predicts a log-law with a higher slope than the Newtonian log-law except at the pipe center where the velocity becomes constant. This behavior is qualitatively in agreement with the experiments although the predictions do not show the double log-law behaviour outside the viscous sub-layer. In none of the predictions the velocity profile coincides with Virk's asymptote especially for the 0.125% PAA in Figure 3-d): here, whereas the experimental data collapse onto Virk's asymptote, the predicted velocities do not but are not too far, especially for M1. Still, the slope of the predicted profile is close to that of the asymptote for M2 and this is consistent with the corresponding friction factor being near Virk's friction factor asymptote (see Figure 1). However, it is also interesting to notice that the corresponding experimental friction factor data do not coincide with the asymptote of Virk for friction.

In some cases, the predictions are in-between the experimental data, i.e., at low y_w^+ the experimental velocities are underpredicted whereas at high y_w^+ they are overpredicted as for the 0.3% CMC solution. For 0.25% CMC the velocity prediction by M1 is better than that of M2 which is consistent with the corresponding friction factor data. The profiles obtained with model M2 are closer to Virk's asymptote than those of model M1 as with the friction factor data.

In our opinion, the absence of the inertial log-law is related to the absence of a region, at high y_w^+ where the damping function assumes a constant value.

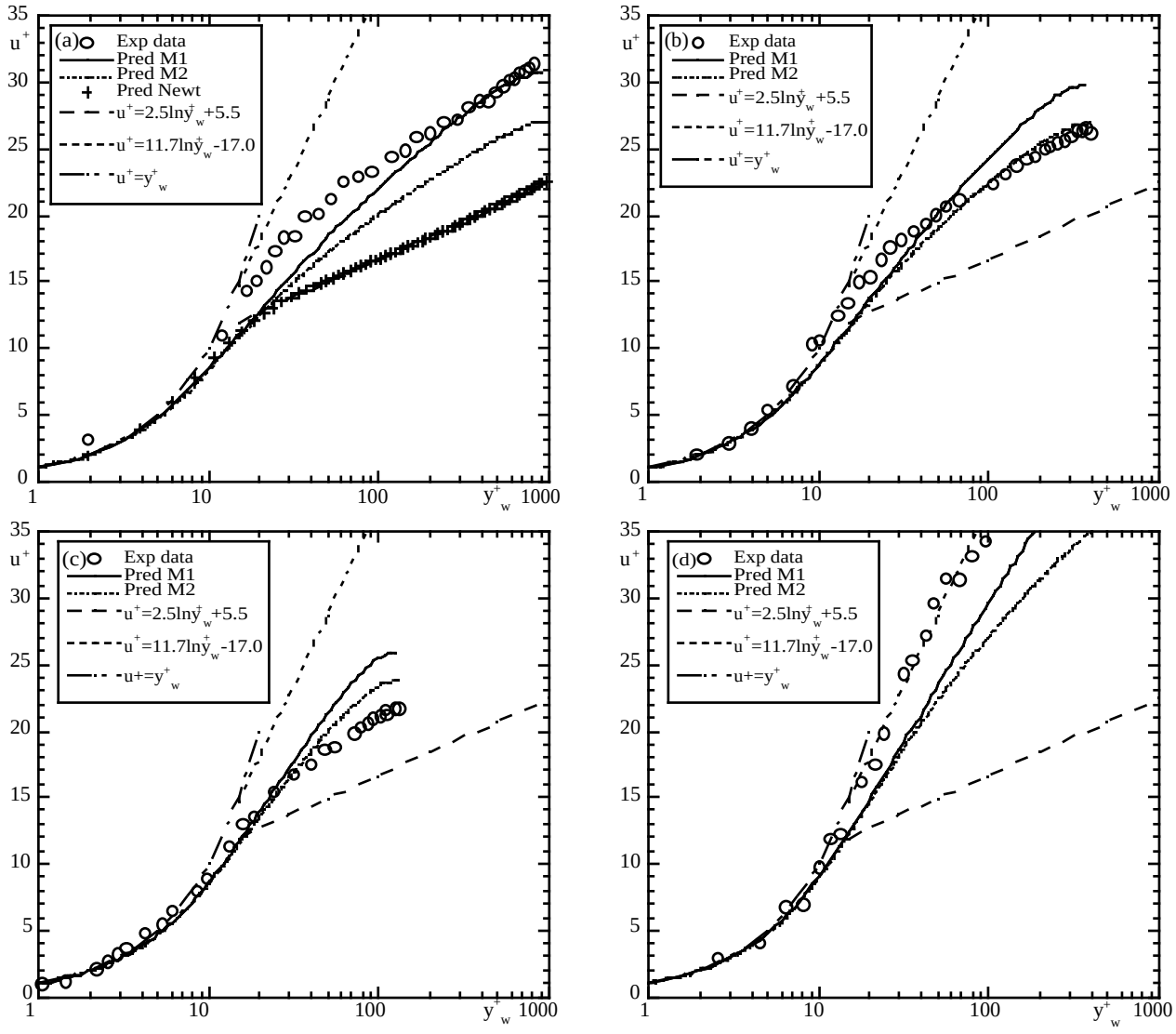

Figure 3- Comparison between calculated and experimental (Escudier et al, 1999) velocity profiles in wall coordinates: (a) 0.09%/0.09% CMC/XG ($Re_w =$ 45300); (b) 0.25% CMC ($Re_w =$ 16600); (c) 0.3% CMC ($Re_w =$ 4300); (d) 0.125% PAA ($Re_w =$ 42900). Newtonian predictions with the same code at $Re_w =$ 200800 (+).

3.4. Turbulent kinetic energy and Reynolds stress profiles

Predictions of k (Figure 4) for 0.125% PAA at $\mathrm{Re}_w = 42970$ are compared with experimental results of Presti (2000). The data from Presti [29] correspond to the same flow conditions as the mean flow data of Escudier et al (1999).

The Newtonian predictions have the expected form with k/u_τ^2 varying from 0 at the wall, going through a maximum of 4.3 at $y_w^+ \approx 20$ and then decreasing towards the axis to a value of 1.25, in agreement with predictions by other Newtonian $k-\varepsilon$ models.

For non-Newtonian fluids both formulations of the turbulence model overpredict turbulence in the central region of the pipe, and the peak turbulence is overpredicted with M1 and underpredicted with M2, except for the PAA in physical coordinates (Figure 4-b). The peak turbulence k/u_τ^2 for drag reducing fluids is always higher than for Newtonian fluids and its location is farther away from the wall (Luchik and Tiederman, 1988). These general features are also captured by the predictions although by different amounts in relation to the experimental data. In several cases the turbulence in the pipe core is well predicted by M2. The peak value of k/u_τ^2 of 12 is probably higher than it should be under drag reducing conditions. Experiments with data on the three components of the normal Reynolds stress are scarce, but amongst the few, Pinho and Whitelaw (1990) found peak values of k/u_τ^2 in excess of 12 for aqueous solutions of CMC, and Presti's (2000) data have maximum values of around 8 except for their polyacrylamide solutions where peak values higher than 12 were also measured.

As far as the location of the peak turbulence is concerned, it is usually overpredicted, the exception being the blend in physical coordinate representation (not shown here). In the inertial layer k^+ is well predicted by M2 for the high

Reynolds number flow cases: XG, the blend and less so the PAA solution. Clearly in excess is also the location of this peak at $y_w^+ = 70$ to 80, which is too far away from the wall, within the inertia dominated region. The higher turbulence peak and its location farther from the wall are features also predicted before by the turbulence models quoted in Section 1 that were adapted for drag reducing flows. In those older turbulence models, peak turbulence was closer to the wall than in here but, as emphasized before, they lacked generality and were previously tuned for the flows to be predicted.

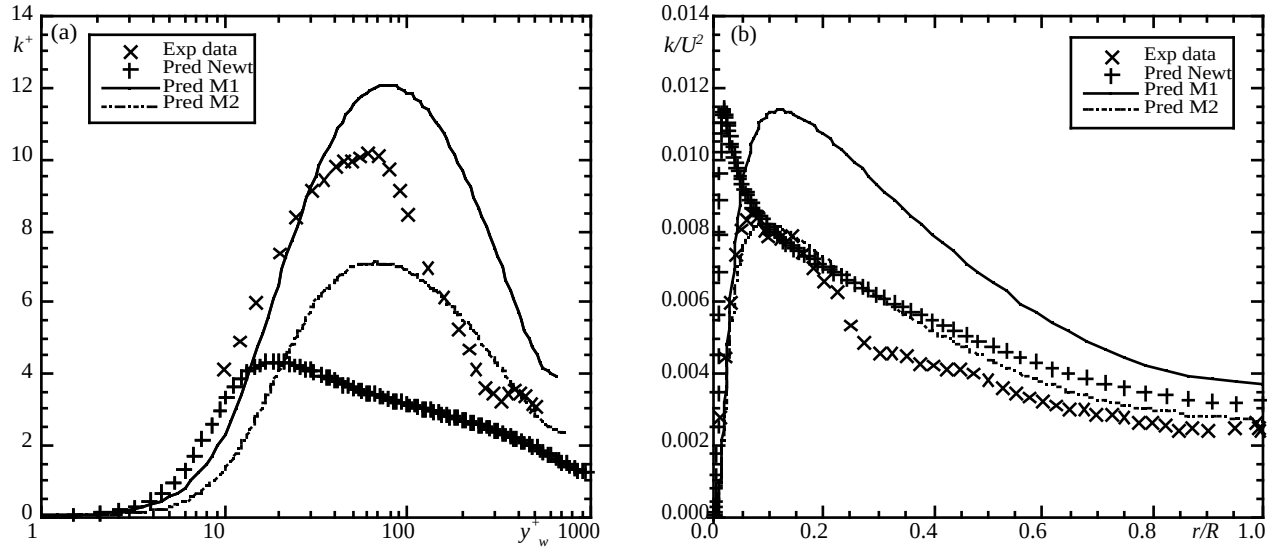

Figure 4- Comparison between calculated and experimental profiles of k at Re_w = 42,900 for 0.125% PAA: (a) wall normalization; (b) physical normalization. Newtonian predictions: Re_w = 42,970.

In terms of k/U^2 the peak turbulence should be lower than for Newtonian fluids, a feature only captured by M2. For the PAA solution the maximum value of k/U^2 of around 0.011 is just less than that of the Newtonian fluid (0.0115), and the peak is located farther from the wall, as it should.

No other experimental data are available in Escudier et al (1999) and Presti (2000), so the following comparisons are between predictions for a Newtonian fluid and for the 0.125% PAA solution.

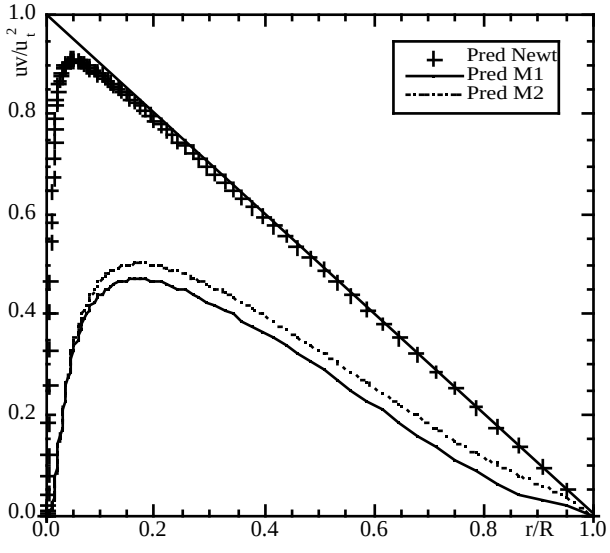

Figure 5- Radial variation of the normalised Reynolds shear stress in pipe flow. Comparison between predictions of Newtonian and 0.125% PAA flows with model 1 (M1) and model 2 (M2) at Re_w = 42,900.

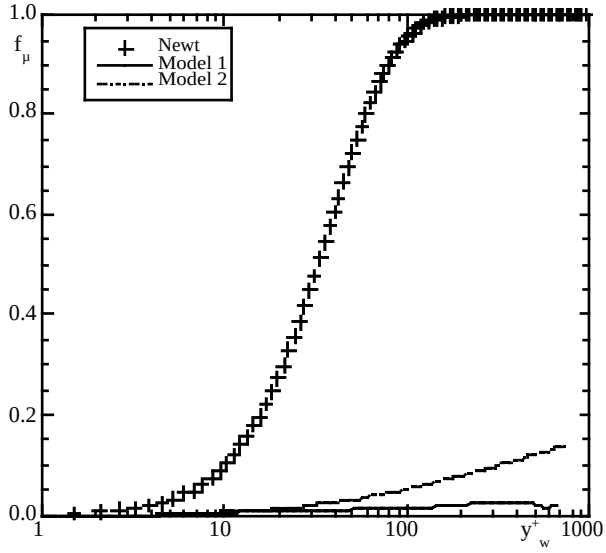

Figure 6- Variation of the damping function f_μ in wall coordinates. Model 1 and Model 2 results obtained with 0.125% PAA.

The radial profiles of Reynolds shear stress $\overline{u'v'}$ are compared in Figure 5. For the Newtonian fluid the shear stress $\overline{u'v'}$ varies linearly in the 80% central region of the pipe in accordance to a momentum balance with negligible

molecular shear stress. However, the 0.125% PAA solution shows a Reynolds shear stress deficit, with M1 predicting the highest deficit in agreement with its higher drag reduction. As far as the peak turbulent shear stress is concerned its location is farther from the wall for the polymer solution, regardless of the damping function adopted and its numerical value is half that for Newtonian fluids. The reasons for this behaviour will become clear next as the radial variations of the damping function f_μ are analysed. The profile of ε, not shown here, shows a maximum for 0.125% PAA that is half the peak Newtonian value, and its location is slightly farther away from the wall than for Newtonian fluids (at $y_w^+ = 10$ against $y_w^+ = 7$ for Newtonian fluids).

These numerical predictions are also qualitatively in agreement with other experimental results (Ptasinski et al, 2001) and with results from DNS simulations of Dimitropoulos et al (2001) using the viscoelastic FENE-P model.

Finally, in Figure 6 the Newtonian, M1 and M2 damping functions f_μ are compared. Whereas the Newtonian f_μ varies from zero at the wall to 1 at $y_w^+ = 300$, the viscoelastic functions are very damping: function M1 does not exceed 0.025 and function M2, although less damping, only reaches a maximum of 0.14.

Since f_μ is also used for the molecular viscosity, (c.f. $f_\nu = f_\mu$ in Eq. 6), the weighted molecular viscosity $\overline{\mu}$ remains basically unaffected by turbulence ($\overline{\mu}_h$) and is given by η_ν. The small decrease of the M1 f_μ at the pipe center is a consequence of the very high local viscosity given by the power law, which was fitted to the intense shear-thinning viscosity behaviour of the 0.125% PAA, since it is the local viscosity that is used to define y^+ (c.f. Eq. 12). By using a constant viscosity to define y_w^+ this feature is removed in the M2 f_μ.

Since the predictions of this turbulence model were adjusted to experimental data by selecting the value of C, the momentum is conserved with the role of $2\mu' s_{ij}$ taken by the purely viscous term $2\overline{\mu} s_{ij}$ and the strong dampening of $\overline{\mu}$ brought by f_ν but this substitution is not equivalent, though. The excessive role played by damping functions f_ν and f_μ are probably undesirable features which were possible here because the adoption of a rheological equation, accounting for the combined effects of shear-thinning, strain-thickening and turbulence on the viscosity, allowed the derivation of the damping functions to be systematic. However, these two strategies are not equivalent in terms of the turbulence model: proper account of $2\mu' s_{ij}$ should reduce the impact of f_μ and f_ν while maintaining the same drag reduction capability, but perhaps affecting favourably the balance between the turbulent quantities $\overline{uv}$, k and ε. This will not free us from the use of damping functions, as is known from Newtonian modeling, but the numerical value of C could probably be reduced.

This constitutes the next major improvement of the present turbulence model. Still, this closure constitutes a breakthrough in the current framework because it is the first model able to predict turbulent drag reducing flows, including the purely viscous case, which only uses as input rheological parameters of the fluid.

4. Conclusions

A low Reynolds number version of the $k-\varepsilon$ model derived in Pinho (2003) was finalised and used to predict turbulent pipe flow of various drag reducing polymer solutions. The model was built on top of the Newtonian model of Nagano and Hishida to which it reduces in the limit of constant viscometric and extensional viscosities. Two new viscous damping functions f_μ and f_ν had to be derived for the new rheological model to take into account wall effects into the eddy and molecular viscosities. The extra term in the dissipation equation was found to have a positive role on turbulent quantities although it had a small effect upon the mean velocity profile and friction factor.

The current turbulence model predicted well the reduction in the friction factor of polymer solutions after quantification of a new model parameter C. Under these conditions, the turbulence model was able to predict satisfactorily mean velocity profiles, the reductions in k, ε and in the production of k, the shift of their peaks away from the wall and the appearance of a deficit in Reynolds shear stress. The damping function recommended is M2 and uses the wall viscosity to compute the wall coordinate y_w^+.

The functions f_μ and f_ν were seen to be too damping probably due to the lack of model for term $2\mu' s_{ij}$ in the momentum equation and solution of this shortcoming constitutes the next major improvement of the model.

5. Acknowledgement

The authors wish to thank CNPq of Brasil and ICCTI of Portugal for funding the exchange programme Project 2001 Proc C 4.3.1. FT Pinho also acknowledges the financial support of FEDER through Fundação para a Ciência e Tecnologia grants POCTI 37699/EQU/2001 and POCTI 37711/EME/2001. We are also in debt to Profs. PJ Oliveira (Universidade da Beira Interior, Portugal), BA Younis (former City University, UK now at U. California, US) and MP Escudier (University of Liverpool, UK) for many valuable discussions. To the latter we are also thankful for making available the turbulent data of Presti (2000).

6. References

Barnes, H.A., Hutton, J.F. and Walters, K. 1989. “An Introduction to Rheology”, Elsevier, Amsterdam.

Cruz, D.O.A., Maneschy, C.E., Macêdo, E.N. and Quaresma, J.N.N. 2000. “A turbulence model for computing the flow of power law fluids within circular tubes” Hybrid Meth. Eng, vol. 2, pp. 1-13.

Cruz, D.O.A. and Pinho, F.T. 2003. “Turbulent pipe flow predictions with a low Reynolds number $k-\varepsilon$ model for drag reducing fluids”. J. Non-Newt. Fluid Mech., in press.

Dimitropoulos, C.D., Sureshkumar, R., Beris, A.N. and Handler, R.A. 2001. “Budgets of Reynolds stress, kinetic energy and streamwise enstrophy in viscoelastic turbulent channel flow” Phys of Fluids, vol. 13, Nº 4, pp. 1016-1027.

Dodge, D.W. and Metzner, A.B. 1959. “Turbulent flow of non-Newtonian systems” AIChEJ, vol. 5, pp. 189-204.

Durst, F. and Rastogi. A.K. 1977. “Calculations of turbulent boundary layer flows with drag reducing polymer additives” Phys of Fluids, vol. 20, pp. 1975-1985.

Escudier, M.P., Presti, F. and Smith, S. 1999. “Drag reduction in the turbulent pipe flow of polymers” J Non-Newt Fluid Mech, vol. 81,pp. 197-213

Hassid, S. and Poreh, M. 1975. “A turbulent energy model for flows with drag reduction” J. Fluids Eng., vol.97, pp 234-241.

Luchik, T.S. and Tiederman, W.G. 1988 “Turbulent structure in low concentration drag reducing channel flows” J. Fluid Mech., vol. 190, pp. 241-263.

Malin, M. R. 1997. “Turbulent pipe flow of power-law fluids” Int. Comm. Heat and Mass Transfer, vol. 24, pp 977-988.

Mizushina, T., Usui, H. and Yoshida, T. 1974. “Turbulent pipe flow of dilute polymer solutions” J. Chem Eng. Japan, vol. 7, pp 162-167.

Nagano, Y. and Hishida, M. 1987. “Improved form of the $k-\varepsilon$ model for wall turbulent shear flows” *J. Fluids Engineering*, vol. 109, pp. 156-.

Patel, V.C., Rodi, W. and Scheuerer, G. 1985. “Turbulence models for near-wall and low-Reynolds number flows: A review” AIAA J, vol. 23, pp. 1308-1319.

Pinho, F.T. and Whitelaw, J.H. 1990. “Flow of non-Newtonian fluids in a pipe” J. Non-Newt. Fluid Mech., vol. 34, pp. 129-144.

Pinho, F.T. 2003. “A GNF framework for turbulent flow models of drag reducing fluids and proposal for a *k*-ε type closure” J Non-Newt. Fluid Mech, in press.

Presti, F. 2000. “Investigation of transitional and turbulent pipe flow of non-Newtonian fluids” PhD Thesis, University of Liverpool, UK.

Ptasinski, P.K., Nieuwstadt, F.T.M., Van den Brule, B.H.A.A. and Hulsen, M.A. 2001. “Experiments in turbulent pipe flow with polymer additives at maximum drag reduction” Flow, Turbulence and Combustion, vol. 66, pp. 159-182.

Van Driest, E.R. 1956. “On turbulent flow near a wall” J. Aeronautical Sci., vol. 23, pp. 1007-1011.

Virk, P.S. 1975. “Drag reduction fundamentals” AIChEJ, vol. 21, pp. 625-656.

7. Copyright Notice